Topological Nonlinear Analysis of Dynamical Systems in Wearable Sensor-Based Human Physical Activity Inference

Yan Yan, *Member, IEEE*, Yi-Chun Huang, Jinjin Zhao, Yu-Shi Liu, Liang Ma, Jing Yang, Xu-Dong Yan, Jing Xiong, *Member, IEEE*, and Lei Wang, *Senior Member, IEEE*

***Abstract*—This work presents a topological nonlinear analysis approach for dynamical system measurements, frequently appearing in sensor-based inference tasks in human physical activity analysis. Traditional approaches to dynamical modeling included linear and nonlinear methods with specific representational abilities and some drawbacks. A novel approach we investigate is using topological descriptors of the shape of the dynamical attractor to represent the nature of dynamics. The proposed framework has three essential advantages compared to previous approaches: 1) with nonlinear phase space reconstruction, the dynamics descriptor is derived from the observation time series without any statistical assumption; 2) with the topological data analysis technique, the phase space topological properties are described in an intrinsic multiresolution analytical way, which brings novel information compared to traditional phase-space modeling techniques; 3) with different types of measurement sensing signals, the proposed approach shows stability in activities state inference. We illustrate our idea with the physical activity recognition tasks with wearable sensors, where the topological characteristics of reconstructed phase state space show strong representational ability for activity type inference.**

***Index Terms*—Dynamical systems, human activity recognition (HAR), nonlinear dynamics, persistent homology, topological data analysis (TDA), topological machine learning.**

Manuscript received 2 November 2022; revised 6 March 2023; accepted 9 May 2023. Date of publication 7 June 2023; date of current version 31 July 2023. This work was supported in part by the National Key Research and Development Program of China under Grant 2020YFC2007200, in part by the Science, Technology and Innovation Commission of Shenzhen Municipality under Grant JSGG20200807171603039, and in part by the International Exchange Program of Chinese Academy of Science and Bulgarian Academy of Sciences. This article was recommended by Associate Editor Z. Wang. *(Y. Yan and Y. Huang contributed equally in this work.) (Corresponding authors: Jing Xiong; Lei Wang.)*

This work involved human subjects or animals in its research. Approval of all ethical and experimental procedures and protocols was granted by the Institutional Review Board/Ethics committees of Shenzhen Institutes of Advanced Technology, Chinese Academy of Sciences under Application No. SIAT-IRB-210715-H0568, and performed in line with the Declaration of Helsinki.

Yan Yan is with the Shenzhen Institute of Advanced Technology, Chinese Academy of Sciences, Shenzhen 518055, China, and also with the Wenzhou Institute of Technology, Wenzhou 325000, China (e-mail: yan.yan@siat.ac.cn).

Yi-Chun Huang is with the Shenzhen Institute of Advanced Technology, Chinese Academy of Sciences, Shenzhen 518055, China, and also with the School of Mechatronic Engineering and Automation, Foshan University, Foshan 528010, China (e-mail: 13104890526@163.com).

Jinjin Zhao is with the School of Biological Science and Medical Engineering, Southeast University, Nanjing 211189, China (e-mail: 220222278@seu.edu.cn).

Yu-Shi Liu, Liang Ma, Jing Xiong, and Lei Wang are with the Shenzhen Institute of Advanced Technology, Chinese Academy of Sciences, Shenzhen 518055, China (e-mail: liuys@siat.ac.cn; liang.ma@siat.ac.cn; jing.xiong@siat.ac.cn; wang.lei@siat.ac.cn).

Jing Yang is with the Shenzhen Institute of Advanced Technology, Chinese Academy of Sciences, Shenzhen 518055, China, and also with the School of Mechanical and Electrical Engineering, Guangzhou University, Guangzhou 510006, China (e-mail: yjde163youxiang@163.com).

Xu-Dong Yan is with the Shenzhen Institute of Advanced Technology, Chinese Academy of Sciences, Shenzhen 518055, China, and also with the Faculty of Data Science, City University of Macau, Macau 999078, China (e-mail: d21091100508@cityu.com).

Color versions of one or more figures in this article are available at https://doi.org/10.1109/THMS.2023.3275774.

Digital Object Identifier 10.1109/THMS.2023.3275774

I. Introduction

HUMAN activity recognition (HAR) has been an essential topic in behavior monitoring, which brought a promising application in healthcare monitoring, pervasive computing, gaming, and entertainment human–machine interaction. The wearable sensor-based sensing systems show superiorities in unrestrained and continuous scenarios like outdoor physical training [1], [2] and daily activity acquiring [3] in healthcare services or intelligent living. Recognizing human physical activities from the on-body sensors is critical for better behavior analysis performance and healthcare service quality improvement. Wearable systems incorporate motion sensors like accelerometers, magnetometers, gyroscopes, or integrated inertial measurement units (IMUs). Modern smartphones, wristbands, or textiles might integrate motion sensors widely available and nonintrusive for users, containing a wealth of information with different types of sensors to be good human activity sensing platforms. Learning from the sensor information to reveal the human activity variation is vital for practical applications.

The sensor signals captured with the wearable sensors can be considered as the observations of the human locomotion dynamical systems. With phase space reconstruction (PSR), the time series can be converted into geometrical objects, including trajectories and state points in the phase state space, which reveal the system's dynamics. Investigating the nonlinear dynamics of sensor signals has achieved fruitful results for physical activity analysis [4], [5], [6], [7], [8]. In dynamical system theory, a phase state space is an abstract space in which all possible system states are represented. Each possible state corresponds to one unique point in the phase state space, representing the dynamics of the nonlinear system. In early studies, the nonlinear dynamics analysis was widely used to study gait variabilities [9], especially in the disease impact [10], [11], injury study [12], sports training [13], and aging problems in human movement [14]. Different

nonlinear dynamics analysis techniques have been previously developed for HAR applications. Frank et al. [4] proposed a geometric template matching (GTM) algorithm, which projects the time series into phase state space. Then the projected data were compared geometrically against their nearest neighbors. Bao et al. [7] explore the GTM algorithm in a 6-D pseudo space to classify actions with Bayesian voting of the k-nearest neighbor classifiers. Saad et al. [5] constructed a nonlinear dynamics analysis framework with the reconstructed phase state space, capturing the dynamical and metric invariants, such as the Lyapunov exponent, correlation integral, and correlation dimension based on the chaos theory. Kawsar et al. [6] developed an HAR approach using the Gaussian mixture models with time-delay embedding and a multisensor body sensing system. Similar work was introduced toward the lightweight smartphone HAR platform in [8]. Tu et al. used the cooperative coevolutionary method [15]. Genetic programming (GP) algorithm [16] toward the PSR optimization. After embedding accelerometer motion sensor data into the phase state space, a 2-D chaotic feature matrix was created with correlation dimension. Maximum Lyapunov exponent of attractor trajectory in the phase state space [17]. These nonlinear features can detect locomotion system variations led by physical activities or disease impact.

Recently, various works have been proposed utilizing topological data analysis (TDA) techniques to infer the human state analysis. For example, Ltindis et al. performed topological EEG analysis to investigate the difference for different motor activity tasks [18] and further explored a comprehensive parameter variation study in EEG applications [18]. Wang et al. [19] validated that the topological features could identify the left temporal region variations and developed a seizure state detection approach. Tlachac et al. explored the audio topological features of depression screening with audio clips from open-ended clinical interviews and scripted crowd-sourced recordings [20]. Saba et al. [21] used the topological barcodes lifetime as a feature toward wheeze detection, similar works performed for preliminary action recognition were introduced in [22] and [23]. The previous illustrated that the different states could be distinguished by exploring the nonlinear dynamics of sensor data with topological analysis.

In this work, we explore the effectiveness and ability of topological nonlinear dynamic descriptors to distinguish between physical activity by acquiring body motion information based on IMU sensors. The topological description approach involves the recently developed TDA tools proposed in the algebra topology area as the state point features in the reconstructed phase state space to discriminate different human activities. The physical activity representative ability validations are performed on sensor-based HAR datasets with a variety of excellences as follows.

1) Better representational ability than other nonlinear/chaotic descriptors.
2) Robustness of sensors both in placement location and sensor types.
3) Small sample learning ability with the topological nonlinear representations. The present work provides an alternative feature set for the sensor-based HAR research community besides the current widely applied time domain, frequency domain, and nonlinear characteristic sets.

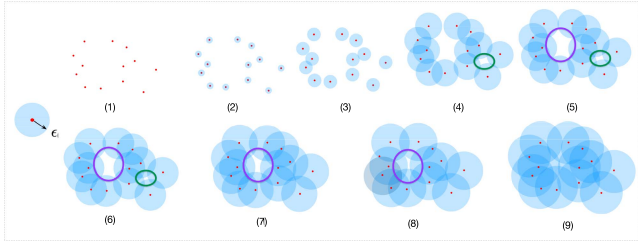

Fig. 1. Homology objects variation illustration with different radius: the touched disks are considered as connected components $\mathbb{H}_0$ while the green and purple circles are the holes $\mathbb{H}_1$.

The rest of this article is organized as follows. We first give preliminary intuition understanding and core notations of TDA in Section II. Then we illustrate the proposed topological inference model by demonstrating sensor-based HAR tasks in Section III. The data materials and experimental settings are allocated in Section IV, and then we present the results and discussion in Section V. Finally, Section VI concludes this article.

II. Preliminaries

A. Overview of Topological Data Analysis

Consider a point cloud set with M points. The TDA technique investigates the underlying space via the following operation and process.

1) First, replace the M points in the point set X with spheres (disks in the 2-D case) with a radius parameter ϵ, i.e., $B(X, \epsilon)$.
2) Then, gradually increase the radius parameter ϵ from 0 to ∞. As the parameter of ϵ gradually increases, the ϵ-spheres collide and merge.
3) Finally, when the radius of the spheres ϵ increases to ∞, all the individual objects of $B(X, \epsilon)$ merged into one single sphere.

As shown in Fig. 1, in the 2-D case, the radius gradually increases from (1) to (9). We can see that the number of topological objects, including *connected components* and *holes*, are different with a different parameter of ϵ. First, we consider the instance of (2) to (3) in Fig. 1 to show the connected component variations. As ϵ increases, four spheres merge, meaning the number of connected components changed from 13 to 11 by two objects disappear. Then consider the hole that exists during (3) to (4) (green circle) in Fig. 1. The variation is also led by the increase of the sphere parameter of ϵ. In the TDA literature, the connected components are denoted as 0-*homology*, and holes as 1-*homology*. Though higher dimensional homology objects are not provided in Fig. 1 due to the 2-D plane limitation, there are higher dimensional homology objects in much higher space. In 3-D space, the 2-homology objects denote loops. In this work, we mainly focus on the information of connected components, holes, and loops denoted as $\mathbb{H}_0$, $\mathbb{H}_1$, and $\mathbb{H}_2$, respectively. The TDA technique investigates the point cloud structure by recording the appear and disappear parameters for each topological object by utilizing *persistent homology* as mentioned in later sections.

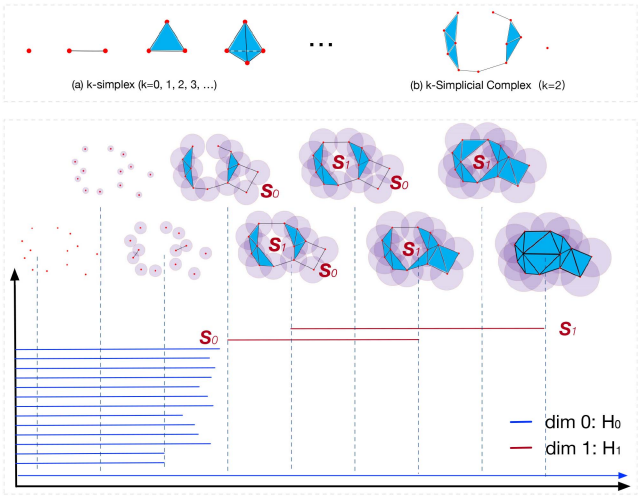

Fig. 2. Topological nonlinear dynamics analysis with sensor signals.

B. Simplicial Complex

The above process can be further described by using the *simplex* and *simplicial complex* objects. For point set $\boldsymbol{X}$ in a space, any subset of a point cloud with cardinality $k+1$ is called a k-simplex [24]. As shown in Fig. 2, the 0-simplices are points, 1-simplices are edges, 2-simplices are triangular faces, and 3-simplices are tetrahedrons. One simplicial complex includes all the lower dimensional simplices and their highest dimension ones. Mathematically, it can be defined as follows.

Definition 1: A simplicial complex $\mathcal{K}$ is a finite collection of simplices, for each simplex σ,

1) any face of $\sigma \in \mathcal{K}$ is also in $\mathcal{K}$, and
2) if $\sigma_1, \sigma_2 \in \mathcal{K}$, then $\sigma_1 \cap \sigma_2$ is a face for both σ_1 and σ_2.

Thus, with different ϵ parameters, the sphere structure developed from the point cloud can be described with the simplicial complex language.

Then for a certain point cloud $\boldsymbol{X}$, it can be naturally converted into a simplicial complex form with the following.

Definition 2: Given a scale parameter ϵ and a point cloud $\boldsymbol{X}$, the Vietoris–Rips complex $\mathcal{K}(\boldsymbol{X}, \epsilon)$ is defined as a simplicial complex contains all subsets with maximum diameter ϵ

$$\mathcal{V}(\boldsymbol{\epsilon}) := \{\sigma \subseteq \boldsymbol{X} | diam\sigma \leq r\}. \tag{1}$$

C. Persistent Homology

Then we reconsider the growing process of ϵ, as shown in Fig. 1. The scale parameter ϵ is a variable ranging from 0 to ∞. With the Vietoris–Rips notation, we denote the origin point cloud as $\mathcal{K}(\boldsymbol{X}, 0)$, and denote the final state when all points merge, as in $\mathcal{K}(\boldsymbol{X}, \infty)$. The persistent homology is proposed by recording the Vietoris–Rips complex while gradually increasing the scale parameter.

Mathematically, consider the growing process with increasing radius parameters $\{\epsilon_0, \epsilon_1, \epsilon_2, \ldots\} \in \boldsymbol{\epsilon}$

$$\mathcal{B}(\boldsymbol{X}, \epsilon_0), \mathcal{B}(\boldsymbol{X}, \epsilon_1), \mathcal{B}(\boldsymbol{X}, \epsilon_2), \mathcal{B}(\boldsymbol{X}, \epsilon_3), \ldots \tag{2}$$

is represented as a sequence of complexes

$$\mathcal{K}(\boldsymbol{X}, \epsilon_0), \mathcal{K}(\boldsymbol{X}, \epsilon_1), \mathcal{K}(\boldsymbol{X}, \epsilon_2), \mathcal{K}(\boldsymbol{X}, \epsilon_3), \ldots \tag{3}$$

Meanwhile, the subsequent Rips complex in the sequence is larger than its previous ones, as *nested*. The nested Rips complex sequence is called a *filtration*, which has the property that

$$\mathcal{K}(\boldsymbol{X}, \epsilon_0) \subseteq \mathcal{K}(\boldsymbol{X}, \epsilon_1) \subseteq \mathcal{K}(\boldsymbol{X}, \epsilon_2) \subseteq \ldots \subseteq \mathcal{K}(\boldsymbol{X}, \epsilon_n) \tag{4}$$

when $\epsilon_0 \leq \epsilon_1 \leq \ldots \epsilon_n$. Thus, for each point cloud embedded from the time series, we have a Vietoris–Rips complex sequence with the varying ϵ, i.e., Vietoris–Rips *filtration*. The theoretical introduction and implementation algorithm of building the Vietoris–Rips complex from the point cloud is described detailedly in [25]. Through tracking the growing process, the homology objects' birth–death ordered pairs are recorded as homology's persistence.

Further, the persistence and birth–death ordered pairs can be visualized using *barcodes*, which track the filtration values of the birth time and death time for the connected components, holes, and loops object in the sequence. As shown examples in Fig. 2, considering the growing process with a 2-D point cloud. The bars in blue color denote the connected components, and the bars in red indicate the holes.

D. Topological Summaries

With the above persistent homology analysis, we can acquire the homology classes and objects with dimensions of 0, 1, and 2, namely, $\mathbb{H}_0$, $\mathbb{H}_1$, and $\mathbb{H}_2$. Consider the number of homology objects in the three dimensions is M, N, P for $\mathbb{H}_0$, $\mathbb{H}_1$, and $\mathbb{H}_2$, respectively. Thus we have three sets to represent the topological features. For $\mathbb{H}_0$, the topological summaries are

$$\left\{\left\{b_0^1, d_0^1\right\}, \cdots \left\{b_0^m, d_0^m\right\}, \cdots \left\{b_0^M, d_0^M\right\}\right\} \tag{5}$$

while for $\mathbb{H}_1$ we have

$$\left\{\left\{b_1^1, d_1^1\right\}, \cdots \left\{b_1^n, d_1^n\right\}, \cdots \left\{b_1^N, d_1^N\right\}\right\} \tag{6}$$

and for $\mathbb{H}_2$ the summaries are represented with

$$\left\{\left\{b_2^1, d_2^1\right\}, \ldots, \left\{b_2^p, d_2^p\right\}, \cdots \left\{b_2^P, d_2^P\right\}\right\}. \tag{7}$$

Thus, the structure information of a specific point cloud is converted into the three ordered pairs with filtration parameters. In this work, we use topological summaries to show the nonlinear dynamics of the human locomotion system when performing different physical activities. Various features built upon the topological summaries have been proposed, including statistical properties, distance analysis, rule-based features, and kernels. In this work, we use the Betti cure (BC) as our topological nonlinear features based on the persistence of $\mathbb{H}_0$, $\mathbb{H}_1$, and $\mathbb{H}_2$, we put the details of BC in the following methodology section.

III. Methodology

A. Overview of the Topological Inference Model in Sensor-Based HAR

In sensor-based HAR tasks, wearable devices capture the inertial information at different human body positions. This work proposes a physical activity recognition framework by characterizing the nonlinear dynamics by topological state point cloud analysis. The collected activity signals are first used to reconstruct the phase state space through time delay embedding. The topological analysis utilizing persistent homology is

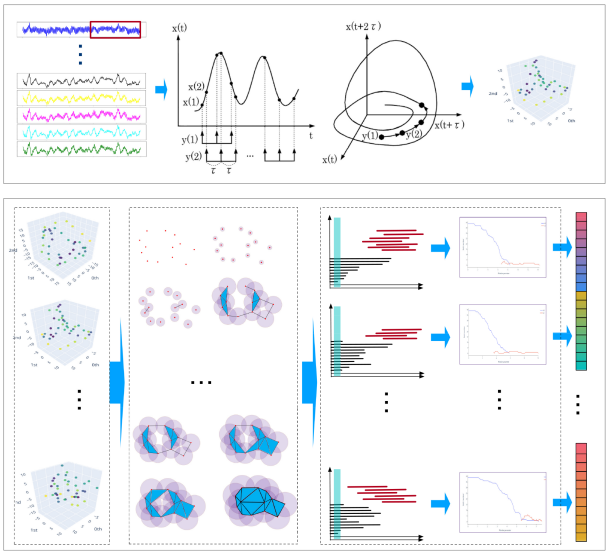

Fig. 3. Topological inference framework with PSR and TDA technique: (up) the preprocessed sensor signals are segmented into multivariate time series, PSR is performed on each channel of signals in the slice; (bottom left) persistent homology analysis of point cloud, with topological summaries extracted; (bottom right) the Betti curves are extracted as the feature vector for one slice with activity category.

performed on each point cloud in the phase state space generated from individual sensor channels. The Betti curve developed from different homology classes is extracted and combined as the feature vector as the activity patterns with the extracted topological summaries. The recognition models are then built with such signal patterns for sensor-based HAR tasks. As shown in Fig. 3, the signals of multisensor channels are first segmented into time series slices with sliding windows. Phase state reconstruction is first individually on each signal in different channels. With the acquired point clouds on each channel, the topological features from all the channels are extracted and combined for further activity type inference.

B. Time Delay Embedding

The state of a deterministic dynamical system is the information required to determine the entire future evolution of the system. The phase state space includes the state points as the set of all possible states of the nonlinear system. The system dynamics are revealed in the phase state space with PSR. The drawn trajectories in the phase state space represent the time evolution, while the points denote the state vector which is undergoing over time [26]. Thus, the phase state space can be used for description of the rules that govern the evolution of the dynamical system.

In this work, we use the delay-coordinate embedding [27], [28] to reconstruct the phase state space. Mathematically, consider the time series of $\{t_0, t_1, \cdots\}$, the delay-coordinate embedding can be denoted as

$$\boldsymbol{x}_k = (t_k, t_{k+\tau}, \ldots, t_{k+(d-1)\tau}) \tag{8}$$

with which the time series is embedded into the points, each denoted as one state vector $\boldsymbol{x} \in \mathbb{R}^d$. Thus we have a state point set of $\boldsymbol{X} = \{\boldsymbol{x}_0, \boldsymbol{x}_1, \boldsymbol{x}_2, \cdots\}$ as the state point cloud which

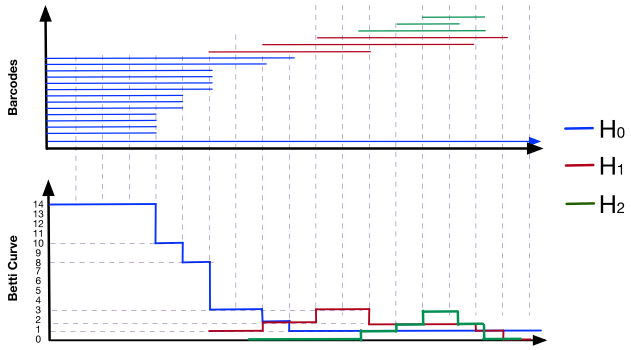

Fig. 4. Betti curves developed from the barcodes as the topological features of sensor signals: the color of blue, red, and green denotes $\mathbb{H}_0$, $\mathbb{H}_1$, and $\mathbb{H}_2$, respectively.

reveals the dynamics of the locomotion system. A demonstration of time delay embedding is shown in Fig. 3, in which the time series is embedded into a 3-D phase state space with the τ as the delay parameter. Two crucial factors in the PSR stage are the time delay parameter denoted as τ and the dimension indicated as d used to unfold the dynamics in the phase state space. We suggest [29] for further discussions on the PSR in nonlinear time series analysis.

C. Topological Feature Extraction

With each point cloud generated by time delay embedding, the persistent homology analysis is performed to extract the topological summaries. In this work, we consider three low-dimensional homology classes of $\mathbb{H}_0$, $\mathbb{H}_1$, and $\mathbb{H}_2$, which denoted the connected components, holes, and loops. The corresponding instances of the topological summaries are illustrated in (5), (6), and (7), respectively. The three sets illustrated all the persistence information in each cloud as the descriptor of the nonlinear dynamics. However, such persistence information cannot be directly used to build models toward further classification and inference problems.

In this work, we use the Betti curve features in the TNDA approach. After achieving the barcodes or persistence diagram of the point cloud, we can map the barcode plot into an integer-valued curve. The process is termed a persistent Betti number (PBN) or Betti curve (BC), which is defined as the summation of all the kth dimensional barcodes

$$f(x, \mathbb{H}_k) = \sum_i \kappa\left(b_k^i, d_k^i\right)(x) \tag{9}$$

in which k denotes the dimension of homology, and i denotes the specific barcode. Thus, for $\mathbb{H}_0$, $\mathbb{H}_1$, and $\mathbb{H}_2$ the corresponding i is ranging in $\{1, 2, \ldots, M\}$, $\{1, 2, \ldots, N\}$, and $\{1, 2, \ldots, P\}$, as the settings in (5), (6), and (7), respectively. The function of κ is a step function, which equals to one in the region $\{b_k^i, d_k^i\}$ and zero otherwise. For instance, as illustrated in Fig. 4, the blue bars of the Barcodes plot are the $\mathbb{H}_0$ objects, where the number decreases from 14 to 10 at the first stage, and finally, only one 0-D exists, as the Betti curve shows. A similar extraction process can be found in $\mathbb{H}_1$ and $\mathbb{H}_2$ cases, denoted in red and green, respectively. We use the mean value of the BC count number of $\mathbb{H}_0$, $\mathbb{H}_1$, and $\mathbb{H}_2$ as our topological feature, which is used as

the classifier's input to build the machine-learning models in our sensor-based HAR applications.

D. Activity Recognition With Different Classifiers

The proposed topological inference approach provides an alternative descriptor for the feature learning tasks in sensor-based HAR. To illustrate the representative ability of the extracted BC features vector, we perform the feature learning experiments developed with several classical classifiers. The Gaussian naive Bayesian (GNB), support vector machine (SVM) classifier with radial basis function (RBF) kernel, k nearest neighbor (kNN), random forests (RF), and multilayer perceptron (MLP) classifiers are used for classification. We evaluate the topological feature learning models on discriminate activity types with several sensor-based HAR datasets. Details of the implementation and experimental settings are provided in the following sections.

IV. Experiments

A. Data Materials

In this work, we mainly consider the activity recognition tasks with the dynamical variation of the human body. Thus, we developed a wearable sensor-based HAR dataset named the TNDA-HAR [30] dataset, in which 50 subjects ranging from 20 to 35, with 25 females and 25 males, are involved in data collection. Five IMU sensors were located at the body's left ankle, left knee, back, right wrist, and right arm. Each IMU sensor contains three types of measurement: the accelerometer, gyroscope, and magnetometer. The sampling rate of the signals was set as 50 Hz. Each subject was required to perform periodic dynamic activities including *static*, *walking*, *running*, *walking up stairs*, *walking down stairs*, and *cycling* (static state includes *sitting*, *laying*, and *standing still* are ignored, but are still provided in the original dataset), each with an acquiring time of 120 s. The dataset is publicly accessible from https://dx.doi.org/10.21227/4epb-pg26 with detailed explanations.

Besides, we also use two other widely used benchmark datasets of the mHealth HAR dataset [31], [32], and the PAMAP2 HAR dataset [33], [34]. These two datasets are also wearable sensor-based and include complete activity annotations. We consider the seven nonstatic activity types of *walking*, *running*, *cycling*, *Nordic walking*, *walking up stairs*, *walking down stairs*, and *roping* in the PAMAP2-HAR dataset, which includes data acquired from nine participants of 24 to 30 years old. The participants wore IMUs on their dominant-side wrist, ankle, and chest, while each IMU contained two 3-D-acceleration sensors, a gyroscope sensor, and a magnetometer sensor, with a sampling frequency of 100 Hz. More details of the dataset can be seen in [31] and [32]. While in the mHealth-HAR dataset, nine nonstatic activities including *walking*, *climbing stairs*, *waist bends forward*, *frontal elevation of arms*, *knees bending*, *cycling*, *jogging*, *running*, and *jumping front back* are used in the experiments, which was collected from ten participants in an out-of-lab environment. Each subject wore wearable sensors attached to the chest, right wrist, and left ankle with a sampling rate of 50 Hz. Further details on the experimental data collection can be found in [33] and [34]. In this work, the signals from the PAMAP2 dataset are first downsampled from 100 to 50 Hz for consistency consideration.

B. Experimental Settings and Model Assessments

For each evaluation, we perform a fivefold cross-validation in this work to perform the model assessment. We use the recognition accuracies, recalls, F1-scores, and confusion matrix for the multiclass classification task to illustrate the accomplished results. For each activity class in the datasets, the predictions of the model were compared to the ground truth labels to calculate the numbers of true-positives (TP), true-negatives (TN), false-positives (FP), and false-negatives (FN). The overall accuracy equals

$$\text{Accuracy} = \frac{\text{TN} + \text{TP}}{\text{TN} + \text{TP} + \text{FN} + \text{FP}} \tag{10}$$

and the precision and recall of one typical class can be calculated by

$$\text{Precision} = \frac{\text{TP}}{\text{TP} + \text{FP}} \quad \text{Recall} = \frac{\text{TP}}{\text{TP} + \text{FN}}. \tag{11}$$

The F1-score is a balanced metric combination of both precision and recall

$$\text{F1-score} = \frac{2 * \text{Precision} * \text{Recall}}{\text{Precision} + \text{Recall}} * 100\%. \tag{12}$$

The average values are used for each experiment's assessment. In addition, several critical confusion matrices are also involved in visualizing the performance of models.

C. Implementation Details

For each dataset, we first perform preprocessing, including signal filtering and normalization, similar to the previous works of literature in dealing with sensor-based HAR datasets. Thus, the continuous time series is then segmented into slices with a temporal size of 128 with an overlapping of 50%, namely, 64 sampling points. Then the multivariate time slices are used for time delay embedding and converted into point clouds. The embedding parameters are set fixed empirically with $d = 5$, $\tau = 5$ in TNDA, $d = 5$, $\tau = 10$ in mHealth, and $d = 5$, $\tau = 10$ in PAMAP2. For the topological feature extraction, we use *giotto-tda* package to perform the building of the Vietoris–Rips complex and the Betti curve feature vector. For the classifiers used in this work,the *scikit-learn* package is used for GNB, SVM-RBF, kNN, RF, and MLP classifier building. Specifically, for kNN classifier, the neighbor parameter is set as 2. For RF classifiers, the estimator's number is set as 46 with bootstrap. For the MLP classifier, the Adam optimization is used with a learning rate of 0.001, the regularization term is L2, and the maximum iteration is 200. The training/testing dataset is divided as 80%/20% for the standard analysis, while the fivefold cross-validation strategy is used for the evaluations. Several more discussion experiments were performed beyond the standard evaluation, and we put the details case by case in the discussion part.

TABLE I
STANDARD TOPOLOGICAL INFERENCE MODEL WITH DIFFERENT CLASSIFIERS IN THREE INVOLVED DATASETS

Dataset	mHealth				PAMAP2				TNDA*			
Metrics	Acc	Pre	Recall	F1	Acc	Pre	Recall	F1	Acc	Pre	Recall	F1
GNB	67.90%	68.01%	69.05%	0.6712	59.71%	66.37%	63.50%	0.5718	66.91%	64.89%	63.26%	0.5945
SVM-RBF	96.94%	96.94%	96.55%	0.9672	90.84%	91.20%	89.53%	0.9006	95.04%	94.73%	94.92%	0.9479
kNN	96.82%	96.89%	95.44%	0.9607	91.96%	92.14%	90.61%	0.9121	95.38%	95.48%	95.41%	0.9554
RF	**97.58%**	**97.52%**	96.80%	**0.9712**	93.04%	92.79%	91.83%	0.9224	95.34%	95.07%	95.29%	0.9516
MLP	**97.58%**	96.61%	**97.11%**	0.9684	**93.96%**	**93.48%**	**92.93%**	**0.9313**	**95.85%**	**95.69%**	**95.79%**	**0.9521**

· Acc denotes the overall accuracies; Pre denotes the average precision; F1 denotes the average mean F1-scores.
· Only the nonstatic activities are involved in this work, the static activity types are ignored.
· Bold font means the best achieved results with the topological inference models developed with five different classifiers.
* Only the three sensors including wrist, ankle, and back sensor signals are used in this experiment with the TNDA-HAR dataset.

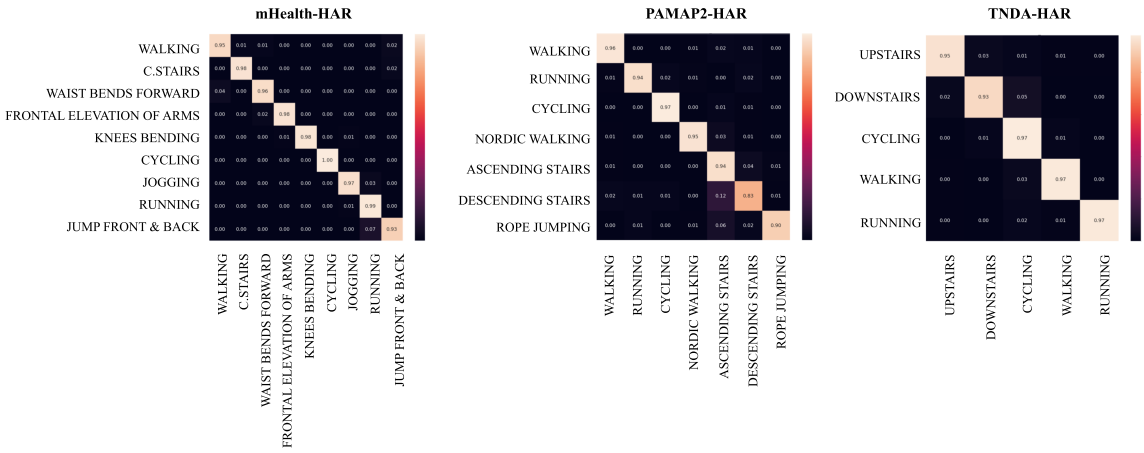

Fig. 5. Confusion matrices of the topological inference model developed with MLP classifier using HAR datasets.

V. RESULTS AND DISCUSSION

A. Sensor-Based HAR With Topological Inference Models

In this work, we consider the recognition problem of some typical physical activities in the sensor-based HAR literature based on three datasets. We use five classical classifiers to implement the topological feature learning models to show the feasibilities and efficiencies.

The results achieved with the topological feature-based learning models are presented in Table I, which include the results classified by the SVM classifier with RBF kernel, Gaussian naive Bayesian, kNN classifier, RF classifier, and MLP classifier. In the mHealth dataset, the best overall accuracy is 97.58% by RF and MLP classifiers; the best recall is 97.11% with MLP classifier; and the best mean-F1 score of 0.9712 by RF-based model. In PAMAP2, the best overall accuracy is 93.96%, the mean recall is 92.93%, and the mean F1-score is 0.9313, achieved by the MLP-based model. In the TNDA dataset with three nine-axis sensors, the best results are 95.85%, 95.79%, and 0.9576 for overage accuracy, average recall, and mean F1-score, respectively.

We can see that the MLP classifier-based model shows best in the multiclass physical activity recognition tasks, with which we illustrate the confusion matrices in Fig. 5. The corresponding details are shown in Table II. However, since the training expense of the MLP classifier is high, we consider using RF classifier in some of the following comparison experiments.

With the presented results above, we can see that the topological inference approach successfully distinguished different physical activities by representing the characteristic of the phase state space. With persistent homology, the structures of the state point clouds are represented and converted into features for classification in sensor-based HAR tasks. The effectiveness is based on two factors: 1) the characteristic ability of PSR; and 2) the representative ability of the TDA. In the following part, we develop validation experiments with corresponding discussions to show how PSR impacts performance and the superiorities of topological inference compared to previous nonlinear descriptors. In addition, the limitations and potential improvements of this work are also provided in the end.

B. Discussion of Topological Inference With Different Number of Sensors

The nonlinear analysis of the dynamical systems utilizing PSR has been widely used in various works of literature. Each time series of the sensor signals can be considered an observation of the nonlinear system, which means that more sensors could provide much more information on the observation of the dynamical system. In this work, we established the TNDA dataset with two different settings of sensor allocation strategy. We consider three experiments from the TNDA dataset denoted as 3S-TNDA, 4S-TNDA, and 5S-TNDA settings, representing physical activity recognition with 3, 4, and 5 wearable sensors, respectively.

TABLE II
TOPOLOGICAL INFERENCE MODEL PERFORMANCE IN SENSOR-BASED HUMAN ACTIVITY RECOGNITION WITH MLP CLASSIFIER

Dataset	mHealth			PAMAP2			TNDA*		
Labels/Metrics	Pre	Recall	F1-Score	Pre	Recall	F1-Score	Pre	Recall	F1-Score
upstairs	-	-	-	78.64%	94.19%	0.8571	97.08%	94.89%	0.9598
downstairs	-	-	-	87.77%	82.84%	0.8524	94.72%	92.58%	0.9364
cycling	100%	100%	100%	98.00%	97.42%	0.9771	91.33%	97.43%	0.9428
walking	96.25%	95.06%	0.9565	97.80%	96.21%	0.9700	97.06%	96.81%	0.9693
running	94.74%	98.90%	.9677	96.48%	94.16%	0.9530	99.58%	96.76%	0.9815
Nordic walking	-	-	-	98.02%	95.27%	96.63%	-	-	-
rope jumping	-	-	-	96.62%	89.94%	0.9316	-	-	-
C. stairs	98.91%	97.85%	0.9838	-	-	-	-	-	-
waist bends forward	96.47%	96.47%	0.9647	-	-	-	-	-	-
frontal elevation of arms	99.00%	98.02%	0.9851				-	-	-
knees bending	100%	98.17%	0.9907	-	-	-	-	-	-
jogging	97.94%	96.94%	0.9744	-	-	-	-	-	-
jumping front & back	86.21%	92.59 %	0.8929	-	-	-	-	-	-
Average	96.61%	97.11%	0.9684	93.33%	92.86%	0.9296	95.69%	95.79%	0.9521
Overall Accuracy		97.58%			93.92%			95.85%	

* Only the wrist, ankle, and back sensor signals are used in this experiment with the TNDA-HAR dataset.
· The corresponding confusion matrices are illustrated in Fig. 5 for the datasets.
· Only the nonstatic activity types involved in all three datasets.

TABLE III
PERFORMANCE OF HAR MODEL WITH TOPOLOGICAL INFERENCE DIFFERENT SENSOR ALLOCATION STRATEGIES

Settings	RF	GNB	SVM	kNN	MLP
3S-TNDA	95.34%	66.91%	95.04%	95.38%	96.02%
4S-TNDA	95.46%	65.93%	95.26%	95.76%	96.43%
5S-TNDA	95.82%	66.94%	96.04%	95.76%	96.76%

TABLE IV
PERFORMANCE OF HAR MODEL WITH TOPOLOGICAL INFERENCE DIFFERENT SENSING MODALITIES

Modality	Accelerometer	Gyroscope	Magnetometer	9-Axis
mHealth	96.31%	96.43%	95.80%	97.58%
PAMAP2	90.09%	90.43%	85.10%	93.04%
3S-TNDA	93.39%	94.45%	91.19%	95.34%
4S-TNDA	93.64%	94.84%	92.08%	95.46%
5S-TNDA	93.95%	94.37%	92.97%	95.82%

The 3S-TNDA experiments include the wrist, ankle, and back IMU sensors; the 4S-TNDA utilize the wrist, ankle, back, and leg IMU sensors; and in the 5S-TNDA case, the wrist, ankle, back, leg, and arm sensors are all included. Here we consider using the RF classifier-based models to perform the comparison, with the overall accuracy value as the multiclass classification performance evaluation. Since most whole-body activity classes are better tracked with multiple sensors (at least three), we ignore the case of a single sensor and two sensors.

As illustrated in Table III, three comparison experiments are proposed, including multiclass activity classification tasks. We can see that with more sensors, the recognition slightly increased with more gathered information from the wearable system. However, in nonlinear dynamical system theory, each of the sensor channels tracks an observation of the human locomotion system. More observations of the system provide more information, which makes a better recognition model. The reason is that the features developed with the characterization of reconstructed space are expanded lead by more sensor signals. Nevertheless, since the sensors had information redundancies when sensors were located too close, the human locomotion system has already been well described by the wrist, ankle, and back sensors. Thus, the improvements are light. Despite the difference led by the difference in the setting of sensor numbers (which are usually located at different positions of the body tracking different kinematics information from the body), the sensor modality is another critical factor, as shown in the following.

C. Discussion of Topological Inference With Different Sensing Modalities

Since the 9-axis IMU sensors usually integrated three different categories of measurements, we set the experiments to show the single modality sensor-based HAR tasks. There are a variety of applications with three-axis accelerometer-based. As illustrated in Table IV, we compare the topological inference models with different sensor modality signals. The nine-axis models significantly outperform the accelerometer-based, gyroscope-based, and magnetometer-based models by the overall accuracy metric. The PSR-based nonlinear dynamics characterization difference also leads to the differences, and the sensor modalities contain independent information by different sensing approaches. Based on the PSR from different sensor modalities, the proposed topological inference approach shows robustness in discriminating the nonlinear dynamics of human activities. Thus, the proposed method provides a flexible feature-learning solution in the applications with only limited modality information available.

TABLE V
PERFORMANCE OF HAR MODEL WITH TOPOLOGICAL INFERENCE WITH SMALL SAMPLE SIZES

Training Set Size	5%	10%	25%	50%	100%
mHealth	97.73%	97.40%	97.32%	97.40%	97.58%
PAMAP2	92.63%	92.52%	92.46%	92.42%	93.04%
TNDA*	95.09%	95.24%	95.14%	95.18%	95.34%

* 3S-TNDA with wrist, ankle, and back sensors.

TABLE VI
AVERAGE ACCURACIES OF TOPOLOGICAL INFERENCE MODEL WITH EXPERIMENTS WITH DIFFERENT SLIDING WINDOW LENGTHS

Window Size	76	102	128 (2.56s)	154	180
mHealth	97.43%	98.27%	96.79%	97.58%	96.88%
PAMAP2	93.85%	94.08%	94.05%	95.05%	94.29%
TNDA*	96.02%	96.18%	96.02%	95.36%	95.66%

* 3S-TNDA with wrist, ankle, and back sensors.

D. Evaluation of Activity Recognition Models With Small Training Sample Set

In this section, we want to validate the effectiveness of the proposed topological inference approach with limited labeled training samples. Based on the experiments of 8:2 of the samples as the portion of training/testing, we further consider the case that uses part of the training set to train the model while keeping the testing set fixed. As illustrated in Table V, we consider the percentages of 5%, 10%, 25%, 50%, and 100% of the training set to show the small sample learning ability. The validation experiments performed on the mHealth, PAMAP2, and TNDA show that the HAR models have insignificant differences in recognition ability with only a small number of training samples. For example, in the first column, when using only 5% of the training set in mHealth, PAMAP2, 3S-TNDA, and 4S-TNDA, the models developed with RF classifier achieved overall accuracies of 97.73%, 92.63%, 95.09%, and 95.33%, respectively. The results have no significant decreasing trend from 97.45%, 92.61%, 95.18%, and 95.43% compared to the last column, which uses 100% of training samples in the 8:2 setting. The robustness of topological features can be integrated into the hybrid, fusion, or deep models in HAR application to improve the representational ability.

E. Robustness Validation With Different Window Length

The PSR process has been performed in a fixed window length of the time slice. It is meaningful to validate the approach's performance in different window lengths. We consider five different window lengths denoted with the number of sampling points of 76, 102, 128, 154, and 180, which denotes a period of 1.52, 2.04, 2.56, 3.08, and 3.6 s, respectively. As shown in Table VI, the results with different window lengths do not significantly reduce average accuracy. The reason is that a longer time series might contain multiple action repetitions with more reconstructed state points, enriching the system's dynamics. Unless the time slice contains less than one cycle of the activity, the topological approach would be able to give a complete description of the locomotion system.

F. Comparison of Activity Recognition Model Performance With Other Nonlinear Descriptors

The robustness of topological features can be integrated into the hybrid, fusion, or deep models in HAR application to improve the representational ability. The proposed approach investigated the topological description of the phase state space as the feature of the human locomotion dynamical system. Various nonlinear features are developed with entropy analysis or geometrical description of phase state space. In this work, the topological point cloud (state point) analysis is proposed as an alternative way to describe the nonlinear dynamics of human locomotion systems in sensor-based HAR problems. A comparison with the previous typical nonlinear descriptors is illustrated in Table VII, including the approximate entropy, sample entropy, phase state space description of the recurrence plot, and Lyapunov exponents. We extract the nonlinear parameters from each signal channel to build the corresponding activity feature vector. Then, we use the RF classifier to perform the HAR tasks with the same settings as in topological inference models. Generally, the topological descriptors of the state point cloud provide better descriptions of the nonlinear dynamics compared to the other involved methods.

The topological approach uses the persistent homology technique to analyze the structure of the state point cloud with multiple space resolutions, which is quite different from the previous geometrical analysis approach. However, such an approach ignores some of the temporal information of the state points reconstructed from the time series. This approach is brought from the geometrical structure description motivation topologically. An improvement in describing the nonlinear system dynamics is to combine the proposed topological structure descriptor with meaningful temporal-related features as one future direction, which is meaningful for the sensor-based HAR tasks because of the inherent temporal properties.

G. Related Work in Sensor-Based Human Physical Activity Recognition

In recent sensor-based HAR studies, the deep learning approaches accomplished significant success in almost every aspect. The proposed approach seeks a novel sensor signal analysis feature that might help improve current frameworks without the ambition to overcome the current state-of-the-art methodologies. However, it is necessary to illustrate how this work differs from modern architecture. Since the activity classes are limited in the proposed TNDA dataset, we here involve the models performed on PAMAP2 and mHealth datasets. We consider the recognition performance with the results of only the used activity types for fair comparisons by reviewing and further calculating based on literature.

For PAMAP2, Wan et al. [35] developed the deep architectures, including convolutional neural networks (CNN), long short-term memory (LSTM) networks, and bidirectional LSTM (BiLSTM) networks, performed on the PAMAP2 dataset, which achieved mean recognition accuracies of 92.01%, 83.89%, and 89.46% for the activity types recognition, respectively. Gochoo et al. [36] performed a feature selection and optimization framework with six groups of features for real-time use, achieving an overall accuracy of 93.77% in the seven activities recognition

TABLE VII
COMPARISON WITH OTHER NONLINEAR DYNAMICS DESCRIPTORS

Dataset	Nonlinear Dynamics Descriptor	Overall Accuracy	Mean Precision	Mean Recall	Mean F1-Score
mHealth (9-class)	Approximate Entropy	96.94%	96.80%	97.27%	0.9702
	Sample Entropy	96.94%	96.90%	97.27%	0.9707
	Recurrence Plot	94.90%	95.06%	95.38%	0.9519
	Lyapunov Exponents	86.15%	86.34%	86.41%	0.8633
	Topological Inference	**97.58%**	**97.52%**	**96.80%**	**0.9712**
PAMAP2 (7-class)	Approximate Entropy	90.27%	90.06%	88.47%	0.8914
	Sample Entropy	90.34%	90.28%	88.47%	0.8925
	Recurrence Plot	86.47%	86.18%	84.30%	0.8506
	Lyapunov Exponents	70.92%	71.57%	65.83%	0.6737
	Topological Inference	**93.04%**	**92.79%**	**91.83%**	**0.9224**
TNDA* (5-class)	Approximate Entropy	94.29%	94.06%	94.21%	0.9409
	Sample Entropy	93.88%	93.63%	93.76%	0.9366
	Recurrence Plot	90.09%	89.67%	89.65%	0.8962
	Lyapunov Exponents	81.78%	81.08%	80.96%	0.8100
	Topological Inference	**95.40%**	**95.13%**	**95.34%**	**0.9512**

* 3S-TNDA with wrist, ankle, and back sensors.
The best-achieved results using the topological inference techniques are shown in bold.

task. Ma et al. [37] proposed AttnSense as a multilevel attention mechanism to recognize human activities, with an average recall of 90.14% in HAR with our similar activities. Challa1 et al. [38] developed a CNN–BiLSTM structure for the HAR tasks with the corresponding recognition mean recall of 93.29%. Gao et al. [39] proposed DanHAR with dual attention network as a deep model, achieving an average recall value of 89.43%.

For the mHealth dataset, Khatun et al. [40] used a deep CNN-LSTM with the self-attention model to distinguish the activities, with a corresponding average recall value of 82.23%. Aljarrah et al. [41] developed a PCA and Bi-LSTM RNN framework for sensor-based HAR with an average accuracy of 96.59% with similar settings. Sarkar et al. [42] proposed spatial attention CNN with a genetic algorithm to perform HAR recognition and achieved an average recall of 99.65%. Zebhi [43] proposed a signal 2-D fast Fourier transform and Wigner–Ville transform-based CNN framework to distinguish different activities, achieving 98.54%, 98.82%, and 98.67% in mean precision, mean recall, and average recognition accuracy, respectively. In this work, the proposed approach achieves comparable performance compared to some of the classical deep learning feature extractors or feature fusion models in distinguishing the nonstatic activity class. However, modern deep learning approaches provide a much more powerful representation than handcraft features. The superiority of the proposed topological features lies in the capability to represent the higher order organization in nonlinear systems, such as the locomotion system in HAR tasks, without heavy training and complex structure.

H. Limitations and Potential Improvements

The main drawback of the proposed framework is the ignorance of the three typical static activity types in most sensor-based HAR studies, including sitting, standing, and laying. The main concern in this work is to investigate human activities from a nonlinear dynamics analysis angle, which shows advantages in describing the geometric structure of the state points. The intrinsic properties of the static activities lack periodic movements, which shows remarkable similarities in their phase state space structure. Such reality brought obstacles for our topological inference approach to distinguish the three statical activities. As shown in Table II and Fig. 5, a similar case happens in the upstairs and downstairs activities that are easily misclassified. They share similar movement patterns, making the state trajectories and point clouds similar in most sensor measurements. However, the proposed topological features are suitable for distinguishing the activity type with significant movements, which expands the modern feature set in sensor-based HAR analysis. Thus, the topological feature set can be incorporated into feature fusion models and deep learning structures to improve the representational ability further.

VI. CONCLUSION

In this work, we proposed a topological scheme for dynamical systems analysis in sensor information inference for human physical activity analysis. In sensor-based HAR applications, human locomotion dynamics are revealed with wearable sensor signals as measurements of nonlinear dynamical systems. Different activities bring different dynamics characteristics described with the topological properties of the state point clouds developed by PSR. The experimental results illustrated that the topological nonlinear analysis approach performs well in distinguishing the state variations in sensor-based HAR tasks proposed in three datasets. Compared to some of the classical nonlinear dynamics descriptors, the topological nonlinear analysis approach shows better representational ability in the sensor-based inference tasks. In addition, the feature-based approach shows robustness in location and modality variation or training sample shortage cases. The topological inference method brings an alternative feature analysis tool toward the inertia signals and activity dynamics analysis.

REFERENCES

[1] Z. Wang, M. Guo, and C. Zhao, "Badminton stroke recognition based on body sensor networks," *IEEE Trans. Human-Mach. Syst.*, vol. 46, no. 5, pp. 769–775, Oct. 2016.

[2] J. Wang, Z. Wang, F. Gao, H. Zhao, S. Qiu, and J. Li, "Swimming stroke phase segmentation based on wearable motion capture technique," *IEEE Trans. Instrum. Meas.*, vol. 69, no. 10, pp. 8526–8538, Oct. 2020.

[3] Z. Wang, D. Wu, J. Chen, A. Ghoneim, and M. A. Hossain, "A triaxial accelerometer-based human activity recognition via EEMD-based features and game-theory-based feature selection," IEEE Sensors J., vol. 16, no. 9, pp. 3198–3207, May 2016.

[4] J. Frank, S. Mannor, and D. Precup, "Activity and gait recognition with time-delay embeddings," in *Proc. AAAI Conf. Artif. Intell.*, 2010, pp. 1581–1586.

[5] S. Ali, A. Basharat, and M. Shah, "Chaotic invariants for human action recognition," in *Proc. IEEE 11th Int. Conf. Comput. Vis.*, 2007, pp. 1–8.

[6] F. Kawsar, M. K. Hasan, R. Love, and S. I. Ahamed, "A novel activity detection system using plantar pressure sensors and smartphone," in *Proc. IEEE 39th Annu. Comput. Softw. Appl. Conf.*, 2015, pp. 44–49.

[7] J. Bao, M. Ye, and Y. Dou, "Mobile phone-based Internet of Things human action recognition for e-health," in *Proc. IEEE 13th Int. Conf. Signal Process.*, 2016, pp. 957–962.

[8] M. O. Gani et al., "A light weight smartphone based human activity recognition system with high accuracy," *J. Netw. Comput. Appl.*, vol. 141, pp. 59–72, 2019.

[9] Y. Yan et al., "Classification of neurodegenerative diseases via topological motion analysis–A comparison study for multiple gait fluctuations," *IEEE Access*, vol. 8, pp. 96363–96377, 2020.

[10] S. Lahmiri, "Gait nonlinear patterns related to Parkinson's disease and age," *IEEE Trans. Instrum. Meas.*, vol. 68, no. 7, pp. 2545–2551, Jul. 2019.

[11] Y. Yan et al., "Topological descriptors of gait nonlinear dynamics toward freezing-of-gait episodes recognition in Parkinson's disease," *IEEE Sensors J.*, vol. 22, no. 5, pp. 4294–4304, Mar. 2022.

[12] C. Strongman and A. Morrison, "A scoping review of non-linear analysis approaches measuring variability in gait due to lower body injury or dysfunction," *Hum. Movement Sci.*, vol. 69, 2020, Art. no. 102562.

[13] S. J. McGregor, M. A. Busa, J. Skufca, J. A. Yaggie, and E. M. Bollt, "Control entropy identifies differential changes in complexity of walking and running gait patterns with increasing speed in highly trained runners," *Chaos: An Interdiscipl. J. Nonlinear Sci.*, vol. 19, no. 2, 2009, Art. no. 026109.

[14] L. Glass, "Synchronization and rhythmic processes in physiology," *Nature*, vol. 410, no. 6825, pp. 277–284, 2001.

[15] R. P. Wiegand, "An analysis of cooperative coevolutionary algorithms," Ph.D. dissertation, George Mason Univ., Fairfax, VA, USA, 2003.

[16] W. Banzhaf, P. Nordin, R. E. Keller, and F. D. Francone, *Genetic Programming: An Introduction*, vol. 1. San Mateo, CA, USA: Morgan Kaufmann Publishers San Francisco, 1998.

[17] P. Tu, J. Li, H. Wang, T. Cao, and K. Wang, "Non-linear chaotic features-based human activity recognition," *Electronics*, vol. 10, no. 2, 2021, Art. no. 111.

[18] F. Altindis, B. Yilmaz, S. Borisenok, and K. Icoz, "Use of topological data analysis in motor intention based brain-computer interfaces," in *Proc. 26th Eur. Signal Process. Conf.*, 2018, pp. 1695–1699.

[19] Y. Wang, H. Ombao, and M. K. Chung, "Topological data analysis of single-trial electroencephalographic signals," *Ann. Appl. Statist.*, vol. 12, no. 3, 2018, Art. no. 1506.

[20] M. Tlachac, A. Sargent, E. Toto, R. Paffenroth, and E. Rundensteiner, "Topological data analysis to engineer features from audio signals for depression detection," in *Proc. IEEE 19th Int. Conf. Mach. Learn. Appl.*, 2020, pp. 302–307.

[21] S. Emrani, T. Gentimis, and H. Krim, "Persistent homology of delay embeddings and its application to wheeze detection," *IEEE Signal Process. Lett.*, vol. 21, no. 4, pp. 459–463, Apr. 2014.

[22] A. Dirafzoon, N. Lokare, and E. Lobaton, "Action classification from motion capture data using topological data analysis," in *Proc. IEEE Glob. Conf. Signal Inf. Process.*, 2016, pp. 1260–1264.

[23] V. Venkataraman, K. N. Ramamurthy, and P. Turaga, "Persistent homology of attractors for action recognition," in *Proc. IEEE Int. Conf. Image Process.*, 2016, pp. 4150–4154.

[24] B. Rieck, "Persistent homology in multivariate data visualization," Ph.D. dissertation, Ruprecht-Karls-Universität, Heidelberg, Germany, 2017.

[25] A. Zomorodian, "Fast construction of the Vietoris–Rips complex," *Comput. Graph.*, vol. 34, no. 3, pp. 263–271, 2010.

[26] J. de Pedro-Carracedo, D. Fuentes-Jimenez, A. M. Ugena, and A. P. Gonzalez-Marcos, "Phase space reconstruction from a biological time series: A photoplethysmographic signal case study," *Appl. Sci.*, vol. 10, no. 4, 2020, Art. no. 1430.

[27] N. H. Packard, J. P. Crutchfield, J. D. Farmer, and R. S. Shaw, "Geometry from a time series," *Phys. Rev. Lett.*, vol. 45, no. 9, 1980, Art. no. 712.

[28] J. C. Robinson, "Takens' embedding theorem for infinite-dimensional dynamical systems," *Nonlinearity*, vol. 12, pp. 1263–1275, 1999.

[29] E. Bradley and H. Kantz, "Nonlinear time-series analysis revisited," *Chaos: Interdiscipl. J. Nonlinear Sci.*, vol. 25, no. 9, 2015, Art. no. 097610.

[30] Y. Yan et al., "TNDA-HAR," *IEEE Dataport*, 2021. [Online]. Available: https://dx.doi.org/10.21227/4epb-pg26

[31] O. Banos et al., "mHealthDroid: A novel framework for agile development of mobile health applications," in *Proc. Int. Workshop Ambient Assist. Living*, 2014, pp. 91–98.

[32] O. Banos et al., "Design, implementation and validation of a novel open framework for agile development of mobile health applications," *Biomed. Eng. Online*, vol. 14, no. 2, pp. 1–20, 2015, Art. no. S6.

[33] M. Arif and A. Kattan, "Physical activities monitoring using wearable acceleration sensors attached to the body," *PLos One*, vol. 10, no. 7, 2015, Art. no. e0130851.

[34] A. Reiss and D. Stricker, "Creating and benchmarking a new dataset for physical activity monitoring," in *Proc. 5th Int. Conf. Pervasive Technol. Related to Assistive Environments*, 2012, pp. 1–8.

[35] S. Wan, L. Qi, X. Xu, C. Tong, and Z. Gu, "Deep learning models for real-time human activity recognition with smartphones," *Mobile Networks Appl.*, vol. 25, no. 2, pp. 743–755, 2020.

[36] M. Gochoo, S. B. U. D. Tahir, A. Jalal, and K. Kim, "Monitoring real-time personal locomotion behaviors over smart indoor-outdoor environments via body-worn sensors," *IEEE Access*, vol. 9, pp. 70556–70570, 2021.

[37] H. Ma, W. Li, X. Zhang, S. Gao, and S. Lu, "AttnSense: Multi-level attention mechanism for multimodal human activity recognition," in *Proc. Int. Joint Conf. Artif. Intell.*, 2019, pp. 3109–3115.

[38] S. K. Challa, A. Kumar, and V. B. Semwal, "A multibranch CNN-BiLSTM model for human activity recognition using wearable sensor data," *Vis. Comput.*, 2021, pp. 4095–4109.

[39] W. Gao, L. Zhang, Q. Teng, J. He, and H. Wu, "DanHAR: Dual attention network for multimodal human activity recognition using wearable sensors," *Appl. Soft Comput.*, vol. 111, 2021, Art. no. 107728.

[40] M. A. Khatun et al., "Deep CNN-LSTM with self-attention model for human activity recognition using wearable sensor," *IEEE J. Transl. Eng. Health Med.*, vol. 10, pp. 1–16, 2022.

[41] A. A. Aljarrah and A. H. Ali, "Human activity recognition using PCA and BiLSTM recurrent neural networks," in *Proc. 2nd Int. Conf. Eng. Technol. Appl.*, 2019, pp. 156–160.

[42] A. Sarkar, S. K. S. Hossain, and R. Sarkar, "Human activity recognition from sensor data using spatial attention-aided CNN with genetic algorithm," *Neural Comput. Appl.*, vol. 35, pp. 5165–5191, 2022.

[43] S. Zebhi, "Human activity recognition using wearable sensors based on image classification," *IEEE Sensors J.*, vol. 22, no. 12, pp. 12117–12126, Jun. 2022.